**Noname manuscript No.**
(will be inserted by the editor)

# Oscillatory Non-normal-Mode Onset of Convection in a Porous Rectangle

**Peder A. Tyvand · Jonas K. Nøland**

Received: date / Accepted: date

**Abstract** A special case of the fourth-order Darcy-Bénard problem in a 2D rectangular porous box is investigated. The present eigenfunctions are of non-normal mode type in the horizontal and vertical directions. They compose a time-periodic wave with one-way propagation out of the porous rectangle. Asymmetry in the horizontal direction generates an oscillatory time-dependence of the marginal state, similar to Rees and Tyvand (2004a). No analytical method is known for this non-degenerate eigenvalue problem. Therefore, the problem was solved numerically by the finite element method (FEM). Three boundaries of the rectangle are impermeable. The right-hand wall is fully penetrative. The lower boundary and the left-hand wall are heat conductors. The upper boundary has a given heat flux. The right-hand wall is thermally insulating. As a result, the computed eigenfunctions show complicated periodic time-dependence. Finally, the critical Rayleigh number and the associated angular frequency are calculated as functions of the aspect ratio, and compared against the case of normal modes in the vertical direction.

## 1 Introduction

Thermal convection in a porous layer uniformly heated from below is known as Darcy-Bénard convection. The linearized onset problem, solved by Horton

P. A. Tyvand
Faculty of Mathematical Sciences and Technology
Norwegian University of Life Sciences
1432 Ås, Norway
Tel.: +47-67231564
E-mail: Peder.Tyvand@nmbu.no

J. K. Nøland (Corresponding Author)
Faculty of Information Technology and Electrical Engineering
Norwegian University of Science and Technology
E-mail: Jonas.K.Noland@ntnu.no

and Rogers [1] and later Lapwood [2], will be referred to as the HRL problem. The fourth-order HRL eigenvalue problem has been thoroughly investigated, but mostly within the framework of normal modes. Normal modes are essentially solutions of a second-order equation, which is the Helmholtz equation. Since the HRL problem is of fourth order, all normal-mode solutions are in principle degenerate solutions of the full fourth-order problem, as pointed out by Tyvand and Storesletten [3]. Tyvand, Nøland and Storesletten [4] designed and solved numerically a 2D problem in a rectangle of the HRL type which is fully non-degenerate, which means that the onset is governed by a non-normal mode solution where the horizontal and vertical dependencies cannot be separated from one another. Such problems cannot be solved fully analytically by known methods, and there will be at least one corner where the sets of thermomechanical boundary conditions at the meeting boundaries are in mutual conflict.

Nield [5] introduced non-normal modes in the vertical direction, solving the HRL problem for all elementary combinations of the Dirichlet or Neumann type for the perturbation temperature and the vertical velocity, where one thermal and one mechanical condition was applied at each boundary. In Nield's work, the solution is automatically a normal mode in the horizontal directions, since a Fourier component for each horizontal eigenfunction expresses normal modes. However, with physical walls confining a rectangular geometry, the solution does not have to be of the normal-mode type, unless wall conditions that give degeneracy are designed. Beck [6] applied normal-mode solutions to the onset problem for 3D rectangular boxes with thermally insulating and impermeable vertical walls. The first analytical solution that did not apply normal modes behavior in one horizontal direction was derived by Nilsen and Storesletten [7], valid for 2D rectangular boxes. These authors had to consider normal modes in the vertical direction in order to make the horizontal eigenvalue problem solvable analytically.

Earlier versions of the HRL problem had only steady onset modes, but Rees and Tyvand [8] designed a 2D problem (the RT problem) for a porous rectangle with oscillatory marginal state induced by an asymmetry between the left-hand and right-hand walls. The RT problem serves as a benchmark problem for our present problem with non-normal-mode eigenfunctions in 2D. The oscillatory onset of the RT problem is represented as a wave that originates at the left-hand wall and travels through the porous box where it exits through the open right-hand wall. The RT problem cannot be solved exactly analytically, since the cell walls for an onset mode have variable spacing, and there exists no critical wave number in the horizontal direction. The solution of the RT problem is well-behaved and has vertical cell walls, which follows from the choice of normal-mode compatible conditions in the vertical direction. Asymptotic solutions for small and large aspect ratios were developed in the RT paper.

The present paper demonstrates high complexity in a HRL eigenvalue problem in 2D, even with simple combinations of either Dirichlet of Neumann conditions at all four walls of a porous rectangle with horizontal and vertical

sides. These eight conditions at four walls are conventionally expressed as one thermal condition and one mechanical condition at each wall.

## 2 Mathematical formulation

A porous medium is considered, with 2D flow in the $x, z$ plane. Its physical counterpart is a 3D porous medium with impermeable and insulating walls $y = 0$ and $y = \Delta y$, where the distance $\Delta y$ is sufficiently small compared with the vertical length scale, implying that the preferred mode of free convection will be 2D in the $x, z$ plane. The $z$ axis is directed vertically upwards. The porous medium is homogeneous and isotropic. The assumption of 2D flow in the $x, z$ plane is valid also for a 3D porous medium with thickness $\Delta y$ in the $y$ direction, if two constraints are met (Storesletten and Tveitereid [12]): (i) The thermomechanical wall conditions at $y = 0$ and $y = \Delta y$ are those of impermeable and thermally insulating walls. (ii) The cell width in the $x$ direction must be sufficiently large compared with $\Delta y$.

The velocity vector $\mathbf{v}$ has Cartesian components $(u, w)$. The temperature field is $T(x, z, t)$, with $t$ denoting time. The undisturbed motionless state has uniform vertical temperature gradient. The gravitational acceleration $g$ is written in vector form as $\mathbf{g}$.

The standard Darcy-Boussinesq equations for convection in a homogeneous and isotropic porous medium can be written

$$\nabla p + \frac{\mu}{K}\mathbf{v} + \rho_0 \beta \ (T - T_0)\mathbf{g} = 0, \tag{1}$$

$$\nabla \cdot \mathbf{v} = 0, \tag{2}$$

$$(\rho c_p)_m \frac{\partial T}{\partial t} + (\rho c_p)_f \ \mathbf{v} \cdot \nabla T = \lambda_m \nabla^2 T. \tag{3}$$

In these equations, $p$ is the dynamic pressure, $\beta$ is the coefficient of thermal expansion, $\rho = \rho_0$ is the fluid density at the reference temperature $T_0$, $\mu$ is the dynamic viscosity of the saturating fluid, $K$ is the permeability, $c_p$ is the specific heat at constant pressure, and $\lambda_m$ is the thermal conductivity of the saturated porous medium. The subscript $m$ refers to an average over the solid/fluid mixture, while the subscript $f$ refers to the saturating fluid alone.

We consider a 2D porous medium with a rectangular shape, bounded by the four sides

$$x = 0, \quad x = l, \quad z = 0, \quad z = h, \tag{4}$$

which means that the 2D rectangular porous box has height $h$ and width $l$.

The lower boundary is taken to be impermeable and perfectly heat-conducting

$$w = 0, \quad T - T_0 = 0, \quad \text{at} \quad z = 0, \tag{5}$$

while the upper boundary is taken to be impermeable and with constant uniform heat flux

$$w = 0, \quad \frac{\partial T}{\partial z} = -\frac{\Delta T}{h}, \quad \text{at} \quad z = h, \tag{6}$$

where $\Delta T$ is the temperature difference across the layer in its undisturbed state. $T_0$ is a reference temperature The left-hand boundary is assumed to be impermeable and perfectly conducting

$$u = 0, \quad T - T_0 = -\frac{\Delta T}{h} z, \quad \text{at} \quad x = 0, \tag{7}$$

while the right-hand boundary is assumed to be (open) fully penetrative and thermally insulating

$$\frac{\partial u}{\partial x} = 0, \quad \frac{\partial T}{\partial x} = 0, \quad \text{at} \quad x = l. \tag{8}$$

This open-wall condition corresponds to a hydrostatic reservoir surrounding the porous medium on the right hand side, combined with a thermal condition of zero heat flux. This combination of kinematic and thermal condition may seem artificial, but it appears as a consistent limit case of the general thermo-mechanical Robin conditions for vertical walls, derived by Nygård and Tyvand [9]. Barletta and Storesletten [10] applied the thermo-mechanical conditions of an open and conducting wall for a vertical cylinder.

### 2.1 Dimensionless equations

From now on we work with dimensionless variables. We reformulate the mathematical problem in dimensionless form by means of the transformations

$$\begin{aligned} &\frac{1}{h}(x,z) \to (x,z), \qquad \frac{h}{\kappa_m}(u,w) \to (u,w), \qquad h\nabla \to \nabla, \qquad \frac{b}{h} \to b, \\ &\frac{1}{\Delta T}(T - T_0) \to T, \qquad \frac{K}{\mu \kappa_m}(p - p_0) \to p, \qquad \frac{(\rho c_p)_f \kappa_m}{(\rho c_p)_m h^2} t \to t, \end{aligned} \tag{9}$$

where $\kappa_m = \lambda_m/(\rho_0 c_p)_f$ is the thermal diffusivity of the saturated porous medium. We denote the vertical unit vector by $\mathbf{k}$, directed upwards.

The dimensionless governing equations can then be written

$$\mathbf{v} + \nabla p - R\, T\mathbf{k} = 0. \tag{10}$$

$$\nabla \cdot \mathbf{v} = 0 \tag{11}$$

$$\frac{\partial T}{\partial t} + \mathbf{v} \cdot \nabla T = \nabla^2 T, \tag{12}$$

with the boundary conditions at the lower and upper boundaries

$$w = T = 0, \quad z = 0, \tag{13}$$

$$w = \frac{\partial T}{\partial z} + 1 = 0, \quad z = 1. \tag{14}$$

The boundary conditions at the vertical sidewalls are

$$u = T - z = 0, \quad x = 0, \tag{15}$$

$$\frac{\partial u}{\partial x} = \frac{\partial T}{\partial z} = 0, \quad x = L. \tag{16}$$

Here $L$ denotes the aspect ratio $L = l/h$. The Rayleigh number $R$ has been introduced. It is defined as

$$R = \frac{\rho_0 g \beta K \Delta T h}{\mu \kappa_m}. \tag{17}$$

### 2.2 Basic solution

The stationary basic solution of eqs. (10)-(14) is given subscript "b"

$$\mathbf{v}_b = 0, \quad T_b = -z, \quad p_b = -\frac{1}{2} R \, z^2. \tag{18}$$

This basic state of hydrostatic fluid has a linear temperature profile.

### 2.3 Linearized perturbation equations

In our stability analysis we disturb the static state (18) with perturbed fields

$$\mathbf{v} = \mathbf{v}_b + \mathbf{v}, \quad T = T_b(z) + \Theta, \quad p = p_b(z) + p'. \tag{19}$$

with perturbations $\mathbf{v}, \Theta, p'$ that are functions of $x, z$ and $t$. Linearizing eqs. (10)-(12) with respect to perturbations and eliminating the pressure gives

$$\nabla^2 w = R \frac{\partial^2 \Theta}{\partial x^2}, \tag{20}$$

$$\frac{\partial \Theta}{\partial t} - w = \nabla^2 \Theta. \tag{21}$$

The onset of convection may occur with a oscillatory marginal state. The only known case where the present configuration of a porous rectangular box is known to give a advected wave solution at marginal stability, was investigated in the RT paper. Here the two vertical end-walls were mutually asymmetric, and none of them were compatible to normal-mode solutions. The unsteady one-way wave process originated as a marginally stable mode at the impermeable/conducting left-hand wall, traveling horizontally through the box, to be transmitted out through the open and thermally insulated right-hand wall. We introduce the streamfunction $\Psi$ by the relationships

$$(u, w) = \left( \frac{\partial \Psi}{\partial z}, -\frac{\partial \Psi}{\partial x} \right), \tag{22}$$

satisfying the continuity equation (11).

### 2.4 The chosen boundary conditions

We first reformulate the above boundary conditions, in terms of the perturbations. The lower boundary is assumed impermeable and perfectly heat conducting

$$\Psi = \Theta = 0, \quad z = 0, \tag{23}$$

while the upper boundary is impermeable, with constant given heat flux

$$\Psi = \frac{\partial \Theta}{\partial z} = 0, \quad z = 1. \tag{24}$$

We have hand-picked boundary conditions at the two sidewalls. The left hand sidewall is impermeable and perfectly heat conducting

$$\Psi = \Theta = 0, \quad x = 0. \tag{25}$$

while the right hand sidewall is partly penetrative and perfectly thermally insulating

$$\frac{\partial \Psi}{\partial x} = \frac{\partial \Theta}{\partial x} = 0, \quad x = L. \tag{26}$$

It is hard to facilitate this condition physically. It may be approached to a reasonable extent by a porous medium made of small metal beads next to a boundary where the medium on the other side of the boundary is made of much larger polystyrene beads. This is a possible configuration for approaching the set (26) of thermo-mechanical conditions, with a saturating fluid with low thermal conductivity, like oil. General Robin conditions for sidewalls have been derived in [9], where the present right-hand wall condition is included as a limit case.

In *Figure* 1 we present a definition sketch in terms of dimensionless variables. Here the four corners of the rectangle are denoted by $O$, $A$, $B$, $C$. Their respective coordinates are $(0, 0)$, $(L, 0)$, $(L, 1)$ and $(0, 1)$. The local eigenfunction fields at the onset of convection behave similarly near each of the two lower corners $O$ and $A$, and also near each of the two upper corners $B$ and $C$. The lower corners $O$ and $A$ have possible local similarities with the analytical solutions from Nilsen and Storesletten [7], see the local analysis below. There are no known analytical solutions relevant for the two upper corners $B$ and $C$.

### 2.5 The coupled differential equations

There are two coupled second-order equations, to be combined with homogeneous boundary conditions for $w$ and $\theta$. We introduce the streamfunction $\Psi$ and rewrite the coupling equations between $\Theta$ and $w$ as

$$\nabla^2 \Theta - \frac{\partial \Theta}{\partial t} = \frac{\partial \Psi}{\partial x}, \tag{27}$$

$$\nabla^2 \Psi + R \frac{\partial \Theta}{\partial x} = Z(z), \tag{28}$$

where the unknown function $Z(z)$ is a constant of integration in the $x$ direction. $Z(z)$ may be evaluated at any value of $x$, and we choose $x = 0$ to find

$$Z(z) = \left(\nabla^2\Psi + R\frac{\partial\Theta}{\partial x}\right)_{x=0} = \left(\frac{\partial^2\Psi}{\partial x^2} + R\frac{\partial\Theta}{\partial x}\right)_{x=0}, \tag{29}$$

applying the boundary conditions (25). From the vertical component of Darcy's law (10) we can rewrite this condition as

$$Z(z) = \left.\frac{\partial^2 p}{\partial x \partial z}\right|_{x=0}. \tag{30}$$

The $x$ component of Darcy's law can be differentiated along the left-hand wall to give

$$\frac{\partial^2 p}{\partial x \partial z} = -\frac{\partial^2\Psi}{\partial z^2} = 0, \quad x = 0. \tag{31}$$

Combining these two conditions at $x = 0$ implies $Z(z) = 0$ which simplifies eq. (28) to

$$\nabla^2\Psi + R\frac{\partial\Theta}{\partial x} = 0. \tag{32}$$

## 3 The eigenfunctions at marginal stability

The eigenfunctions $\Psi(x, z, t)$ and $\Theta(x, z.t)$ for the onset of convection have separable time dependence and can be rewritten as

$$(\Psi, \Theta) = (\psi(x, z), \theta(x, z))e^{\sigma t}, \tag{33}$$

where the complex growth rate $\sigma = \sigma_r + i\sigma_i$ has been introduced, and $i$ denotes the imaginary unit.

The coupled governing equations can now be written

$$\nabla^2\theta - \sigma\theta = \frac{\partial\psi}{\partial x}, \tag{34}$$

$$\nabla^2\psi + R\frac{\partial\theta}{\partial x} = 0, \tag{35}$$

with the boundary conditions

$$\psi = \theta = 0, \quad z = 0, \tag{36}$$

$$\psi = \frac{\partial\theta}{\partial z} = 0, \quad z = 1, \tag{37}$$

$$\psi = \theta = 0, \quad x = 0, \tag{38}$$

$$\frac{\partial\psi}{\partial x} = \frac{\partial\theta}{\partial x} = 0, \quad x = L. \tag{39}$$

Marginal stability is defined by $\sigma_r = 0$, while a nonzero angular frequency $\omega$ may appear, defined as $\omega = \sigma_i$. It will arise as a new eigenvalue in the

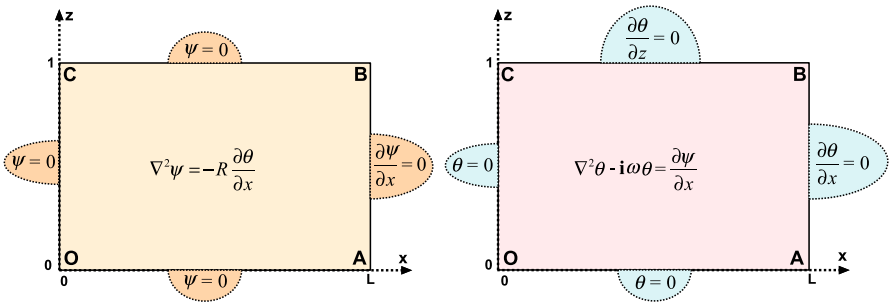


**Fig. 1** Illustration of the governing equations and corresponding boundary conditions of the coupled eigenvalue problem.

problem, which may also cause the eigenfunctions to be complex, with real and imaginary parts defined as

$$\psi(x,z) = \psi_r + i\psi_i, \qquad \theta(x,z) = \theta_r + i\theta_i. \tag{40}$$

The governing equations can now be split in real and imaginary parts as follows

$$\nabla^2\theta_r + \omega\theta_i = \frac{\partial\psi_r}{\partial x}, \tag{41}$$

$$\nabla^2\theta_i - \omega\theta_r = \frac{\partial\psi_i}{\partial x}, \tag{42}$$

$$\nabla^2\psi_r + R\frac{\partial\theta_r}{\partial x} = 0, \tag{43}$$

$$\nabla^2\psi_i + R\frac{\partial\theta_i}{\partial x} = 0. \tag{44}$$

The full solution for the marginal state of convection must be found numerically, since no analytical solutions are known for this fourth-order eigenvalue problem without degeneracies in 2D. No Fourier methods are known, but in principle a double power series solution in terms of $x$ and $z$ could be attempted. It would at best converge slowly, so a finite element method is a better alternative. We use the commercial finite-element package Comsol Multiphysics.

### 3.1 Local quasi-steady approximations for the eigenfunctions

We will develop analytical approaches concerning the eigenfunctions in the vicinity of two of the four corners of the porous rectangle. These are based on earlier work where the onset of convection is non-oscillatory, and may be valid as first approximations only asymptotically as $L \gg 1$.

*3.1.1 Local flow near* $(0,0)$

The first corner that we consider is the origin $O$, with coordinates $(0,0)$. The local behavior of steady-state eigenfunctions can be deduced from Nilsen and Storesletten [7], see also Rees and Tyvand [11]. Their solution has a degeneracy which implies the existence of two different candidates for local solutions, which we call alternative $A1$ and alternative $A2$, when applied to the flow around the origin. We are only interested in the local spatial dependency of the eigenfunctions, so we disregard the relative (complex) amplitudes of the temperature perturbation versus the streamfunction.

**Alternative A1**
The first alternative for possible local quasi-steady eigenfunctions around the corner $O$ is

$$\begin{aligned} \theta &\sim \sin(kx)\sin(\alpha x)\sin(mz), \\ \psi &\sim \cos(kx)\sin(\alpha x)\sin(mz). \end{aligned} \tag{45}$$

The local Taylor expansions for eq. (45), representing alternative $A1$, are given by

$$\begin{aligned} \theta &\sim x^2 z + O(x^2 z^3), \\ \psi &\sim xz + O(xz^3) + O(x^3 z), \end{aligned} \tag{46}$$

and we note the qualitative difference between the eigenfunctions: The perturbation temperature has zero normal derivative at the wall $CO$ ($x = 0$), while there is a finite vertical velocity along this wall. In the plots below, this alternative will show relatively great spacing between neighboring isotherms near the wall $CO$, and there will be a relatively smaller distance between neighboring streamlines near the same wall $CO$. A more precise way of making comparisons between our numerical solutions and these local quasi-steady solutions (46), is to introduce what we call the Local Gradient Angle (LGA), denoted by $\gamma$. The angle $\gamma$ is defined as the angle between the $x$ axis and the direction where the local gradient of an eigenfunction intersects the origin. *Figure* 2 shows an intuitive illustration of the LGA concept, since it corresponds to the direction where a ray of light emitted from the origin is reflected back (with the isotherm acting as a mirror surface) along the same direction as it came from, while all other rays directed differently will be scattered from this surface.

For defining the LGA for the temperature perturbation, we thus require the gradient and the position vector to be parallel

$$\left(\frac{\partial\theta}{\partial x}, \frac{\partial\theta}{\partial z}\right) \times (x, z) = 0. \tag{47}$$

We now assume the temperature perturbation to have a general power dependency of $x$, taking the local expansion with respect to $O$ as

$$\theta \sim x^n z, \tag{48}$$

since the linear $z$ dependence is known because of antisymmetry with respect to the $x$ axis. This assumed $z$ dependency does not have to be a Taylor expansion, since it has no physical meaning to extend an eigenfunction on the other side of the $z$ axis. From the definition (47) and the assumed local field (48) we find the relationship between the LGA and its exponent $n$

$$n = \cot^2 \gamma, \tag{49}$$

since $\tan \gamma = z/x$.

The present alternative A1 thus determines the LGA as $\gamma = \arctan(2^{-1/2})$, for the temperature perturbation. The local solution for the streamfunction is simpler, since it is symmetric in $x$ and $z$, implying that the local gradient that goes through the origin has the ratio $z/x = 1$ and makes an angle $\pi/4$ with the $x$ axis.

**Alternative A2**

A particular degeneracy of the steady local corner problem implies that streamlines and isotherms can be interchanged. Therefore there is a second alternative $A2$ for possible local eigenfunctions around the corner $O$, given as

$$\begin{aligned} \theta &\sim \cos(kx)\sin(\alpha x)\sin(mz), \\ \psi &\sim \sin(kx)\sin(\alpha x)\sin(mz). \end{aligned} \tag{50}$$

The corresponding local Taylor expansions for eq. (50), representing alternative $A2$, are

$$\begin{aligned} \theta &\sim xz + O(xz^3) + O(x^3 z), \\ \psi &\sim x^2 z + O(x^2 z^3). \end{aligned} \tag{51}$$

which means that alternative $A2$ interchanges the roles of the eigenfunctions in alternative $A1$. This means that the LGA for $\theta$ is $\gamma = \pi/4$, while the LGA for $\psi$ is $\gamma = \arctan(2^{-1/2})$. In the plots below, this alternative may reveal itself by having a small distance between neighboring isotherms near the wall $CO$, and a relatively greater distance between neighboring streamlines near the wall.

These one-term local expansions require $|x| \ll 1$ and $0 < z \ll 1$. The three wave numbers $(k, m, \alpha)$ that are present in the mathematical solution by Rees and Tyvand [11], lose their significance to the leading order of the Taylor series, since they do not affect the shapes of the eigenfunctions. The degeneracy that is responsible for the two distinct alternatives of eigenfunctions, exist because of the wave number of degeneracy $\alpha$, which is determined by a Helmholtz equation.

The numerical solution may determine which of the two quasi-steady candidates (45) and (50) for local eigenfunctions that are actually represented near the origin at marginal stability. However, it is more probable that none of these alternatives (with a precise integer exponent, either $n = 1$ or $n = 2$) is chosen, since the exact problem has only one solution. The numerical solution

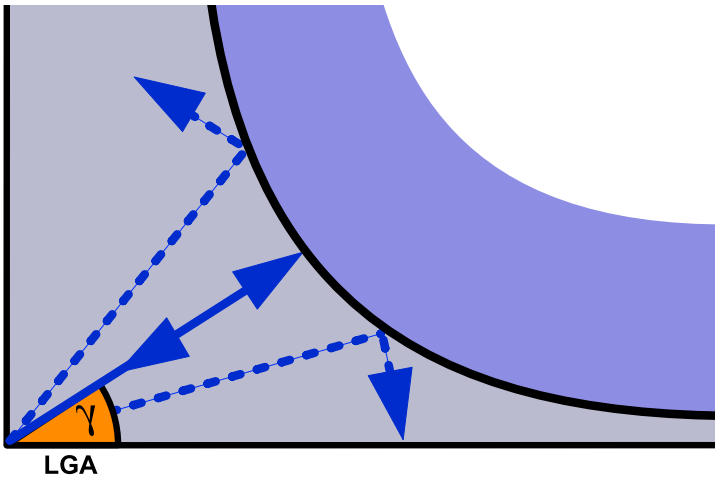


**Fig. 2** Illustration of our concept of "local gradient angle" (LGA), giving the direction of the local gradient vector that points through the origin. This concept characterizes a family of local scalar fields $(x^n z)$, here visualized by a ray of light emitted from the origin and reflected back from the isoline $x^n z$ =constant. The only ray that is reflected back to the origin is aligned along the local gradient angle. The case given in this figure is n=2.

is not likely to switch between two alternatives of quasi-steady local solutions, since two distinct alternatives will no longer exist once we allow oscillations to enter the problem. We also note that a superposition of the two local quasi-steady solutions is not an option, since it does not give a converging value for the LGA. The LGA and its exponent $n$ as defined by eq. (49) will illustrate the behavior of the local solution during an oscillation period.

### *3.1.2 Local flow near* $(L, 0)$

The local behavior of the quasi-steady eigenfunctions near the second corner $A$ (with coordinates $(L, 0)$) is similar to the behavior at the origin $O$. The basic difference is that we have let the previous expressions for the eigenfunctions apply to their $x$ derivatives, after having made the coordinate substitution $x \to (x - L)$.

**Alternative A3**
The first alternative for possible local eigenfunctions around the corner $A$ is

$$\begin{aligned} \frac{\partial \theta}{\partial x} &\sim \sin(k(x-L))\sin(\alpha(x-L))\sin(mz), \\ \frac{\partial \psi}{\partial x} &\sim \cos(k(x-L))\sin(\alpha(x-L))\sin(mz). \end{aligned} \tag{52}$$

The local Taylor expansions for eq. (52), representing alternative $A3$, are given by

$$\begin{aligned} \frac{\partial\theta}{\partial x} &\sim (x-L)^2 z + O((x-L)^2 z^3), \\ \frac{\partial\psi}{\partial x} &\sim (x-L) z + O((x-L) z^3) + O((x-L)^3 z), \end{aligned} \tag{53}$$

and we note the qualitative difference between the eigenfunctions. The local streamlines will go perpendicularly out through this wall, with zero temperature gradient.

**Alternative A4**

The degeneracy of this local corner problem implies that streamlines and isotherms can be interchanged. Therefore there is a second alternative $A2$ for possible local eigenfunctions around the corner $A$, given as

$$\begin{aligned} \frac{\partial\theta}{\partial x} &\sim \cos(k(x-L)) \sin(\alpha(x-L)) \sin(mz), \\ \frac{\partial\psi}{\partial x} &\sim \sin(k(x-L)) \sin(\alpha(x-L)) \sin(mz). \end{aligned} \tag{54}$$

The corresponding local Taylor expansions for eq. (54), representing alternative $A4$, are

$$\begin{aligned} \frac{\partial\theta}{\partial x} &\sim (x-L) z + O((x-L) z^3) + O((x-L)^3 z), \\ \frac{\partial\psi}{\partial x} &\sim (x-L)^2 z + O((x-L)^2 z^3), \end{aligned} \tag{55}$$

which means that alternative $A4$ interchanges the roles of $\theta$ and $\psi$ in alternative $A3$.

### *3.1.3 On the troublesome corners* $(L,1)$ *and* $(0,1)$

The local thermomechanical solution near the third corner $B$ (with coordinates $(L,1)$) will not be analyzed here. $B$ is a troublesome corner, together with the fourth corner $C$. The two sides that meet in the corner $B$ ($AB$ and $BC$) have boundary conditions incompatible with normal modes, and the solution may be singular in the corner $B$. At an infinitesimal distance from the corner $B$, it is hard to tell whether the streamlines are normal or parallel to one another. Near the corner $C$ the situation is similar.

## 3.2 Numerical solutions

We have now discussed the four corners, with a warning of possible singularities in the corners $B$ and $C$. If so, the numerical solution may represent the outer solution in the sense of matched asymptotics, with respect to the corners $B$

and $C$. The solution will be well-behaved around the two other corners $O$ and $A$ of the rectangle, where there are no conflicting boundary conditions. In fact, the two eigenvalues $R$ and $\omega$ have to be solved simultaneously. The solution is found by iterations with respect to the growth rate $\sigma_r$, in order to achieve a valid result that fulfills $\sigma_r = 0$ with sufficient accuracy. The imaginary part that arises numerically for the eigenvalue $\omega$, is equal to $-\sigma_r$. The numerical search is based on an optimization problem to be solved, where the solver finally picks the correct $\omega$ to reach an imaginary part $(-\sigma_r)$ less than $10^{-5}$.

#### *3.2.1 The porous square* ($L = 1$)

The natural start is the square domain, which is displayed in *Figure* 3. The four eigenfunctions with the lowest Rayleigh numbers are shown. In each case, five snapshots of the eigenfunctions are displayed, representing half an oscillation period. The isotherms are represented by solid black lines, supported by color coding. The streamlines are conveniently represented by white graphs on the colored background. There are constant intervals in the displayed values of the perturbation temperature and streamfunction.

The preferred mode for convection has a critical Rayleigh number $R = 60.49$, which is more than 50% above the classical value of $4\pi^2$ (Horton and Rogers [1]). We observe the curved thermal cell walls, while the flow cells have internal cell walls that are not so far from being vertical. For the higher onset modes, we observe curved cell walls both horizontally and vertically. The third and fourth onset modes develop recirculating domains within greater structures that defy the notion of a convection cell, which should not come as a surprise since there exists no wave number concept in these cases. These recirculating flow domains tend to be surrounded by wavy flows that are unidirectional along the lower and upper boundary of the porous layer.

#### *3.2.2 A narrow porous domain* ($L = 0.5$)

*Figure* 4 shows the four eigenfunctions with the lowest Rayleigh numbers for a narrow rectangle with the aspect ratio $L = 0.5$. The curvatures in the internal cell walls are more pronounced compared with *Figure* 3. The fourth set of eigenfunctions reveal the tendency that recirculating domains (with closed isolines for the temperature perturbation or the streamfunction) are surrounded by wavy isolines that do not close, but extend through the entire horizontal width of the rectangle, following the lower and upper boundary. Interestingly, this situation changes during an oscillation period as far as the isotherms are concerned: The isolines for the perturbation temperature forms closed cells during parts of an oscillation period, while these cells open up by shearing their outer isotherms during other parts of an oscillation period.

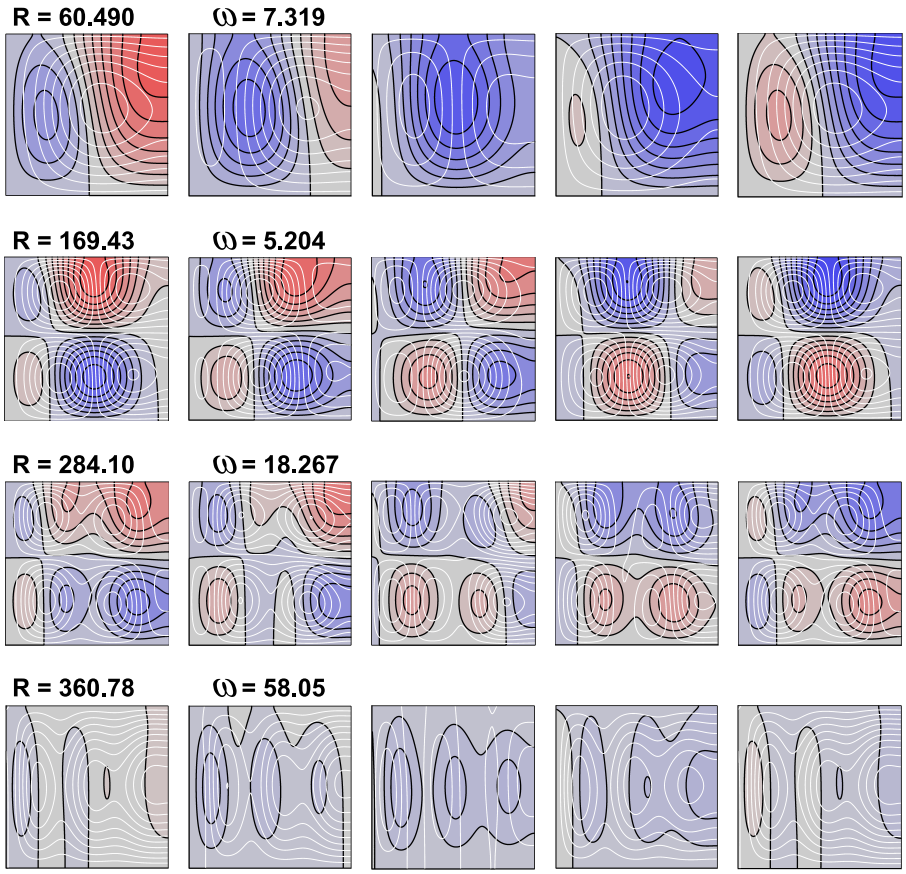


**Fig. 3** Streamlines (white) and isotherms (black) at equally spaced time intervals over one-half of a period for convection in a square (aspect ratio $L = 1$) for the 4 first eigenfunctions. Time increases from the left to the right.

### *3.2.3 A moderately wide porous domain* ($L = 2$)

We will now show numerical results for the case $L = 2$. We first recall some known analytical results for $L \gg 1$. The case of infinite width with the present conditions for the lower and upper boundaries, was studied by Nield [5], who established the critical Rayleigh number, with associated wave number and critical frequency

$$Ra_c = 27.10, \quad \alpha_c = 2.33, \quad \omega_c = 0, \tag{56}$$

and these are asymptotic limits to be approached as $L \to \infty$. The oscillation vanishes in the asymptotic limit as $L \to \infty$, which is known from Nield [5].

*Figure* 5 shows how the LGA varies over an oscillation period. *Figure* 6 shows the associated variation of the LGA exponent $n$ during a period of oscillation, found by inserting the computed values of $\gamma$ in eq. (49). The relevance

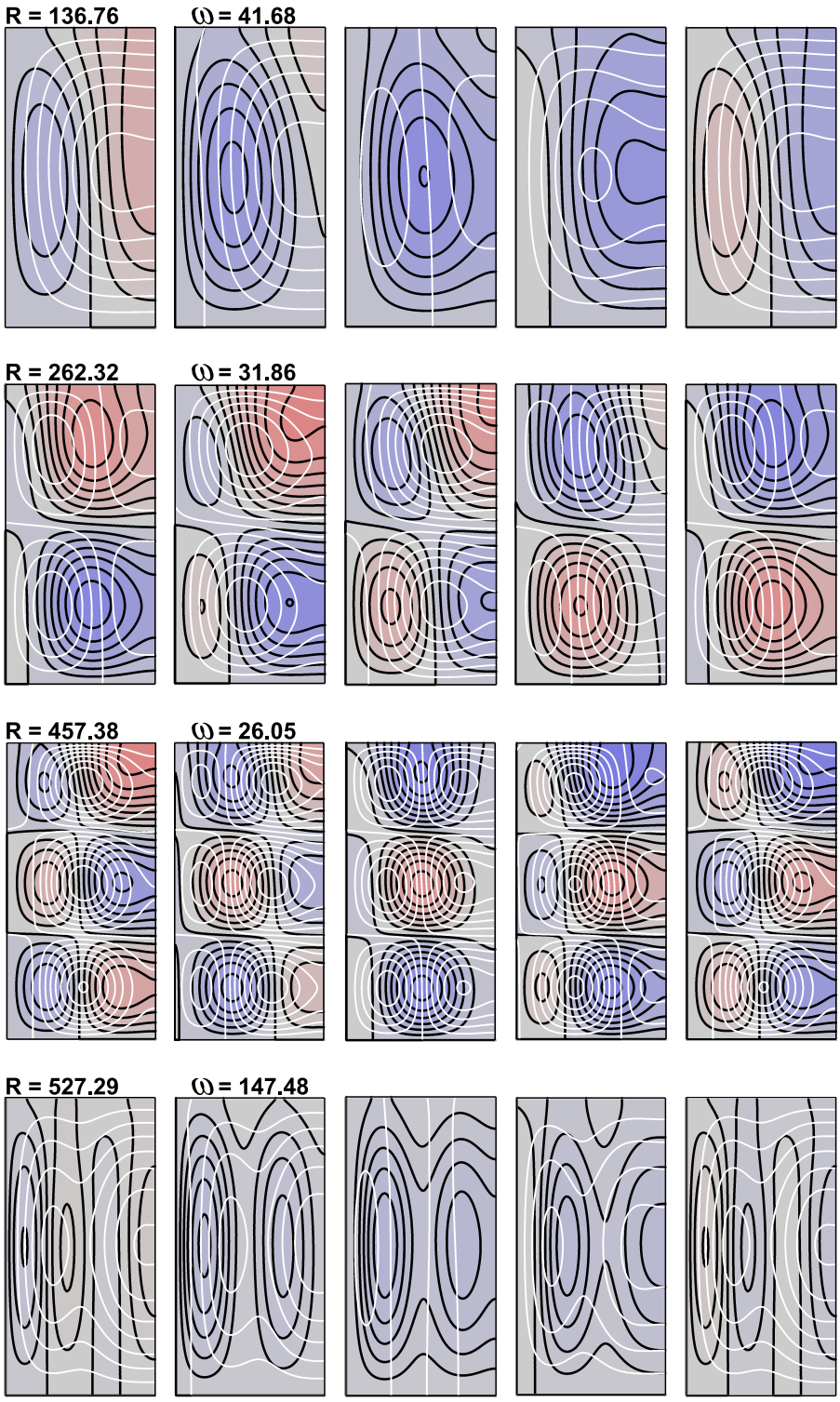


**Fig. 4** Streamlines (white) and isotherms (black) at equally spaced time intervals over one-half of a period for convection in a narrow reactance (aspect ratio $L = 0.5$) for the 4 first eigenfunctions. Time increases from the left to the right.

of one discrete value $n = 1$ appearing in our above quasi-steady local solutions is seen in *Figure* 6, since it will give a reasonable approximation to one of the two eigenfunctions. The other discrete value $n = 2$ will not have a similar role, but most of the higher values of $n$ will be confined to the interval between 1 and 2. Our numerical results confirm the expectation that the leading $x$ dependency near the origin cannot be represented as a Taylor expansion around $x = 0$, as the series is one-sided only, requiring $x > 0$. Our non-singular local solution with a non-integer exponent for $x$ puts the eigenfunction degeneracy found by Nilsen and Storesletten [7] in a broader perspective. Their results were confirmed by Rees and Lage [13] and later generalized by Rees and Tyvand [11].

*Figures* $5-6$ show exactly the same behavior for both eigenfunctions over an oscillation period, but their respective phase shift is not $\pi/2$ as one might expect. This asymmetry in phase shifts between the eigenfunctions implies that the LGA exponent $n$ for the temperature field will exceed the value of $n$ for the streamfunction for more than half of the oscillation period. We offer no explanation for the remarkable discontinous jumps of the LGA that happen twice during the oscillation period both for the temperature and the streamfunction.

*Figures* $5-6$ represent the preferred eigenfunctions for flow and temperature, having the lowest Rayleigh numbers. Isolines for these preferred eigenfunctions are shown in *Figure* 7. Here we consider a moderately wide rectangle with the aspect ratio $L = 2$. Still the lowest eigenvalue, $R = 36.553$, is much higher than the the limit value 27.10 for an infinitely wide rectangle. There is a significant stabilizing effect of the wall $AB$ where buoyancy is taken away due to zero temperature perturbation. There is still no critical wave number concept that can be extracted from the results for $L = 2$. The eigenfunctions for $L = 2$ show interesting combinations of cells that close next to cells that do not close, both for the streamlines and the isotherms. *Figure* 7 shows flow cells that do not split in the vertical direction.

In addition, *Figure* 8 illustrates the third and fourth eigenfunctions, ranked according to the Rayleigh number, for the aspect ratio $L = 2$ (same as *Figure* 7). Considering the fourth eigenvalue of the Rayleigh number, an almost horizontal cell wall arises near the middle of the porous layer, and it is approximately a joint cell wall for the streamlines and the isotherms. In fact, the intricate relationships between streamlines and isotherms seems to be outside the reach of analytical solutions. They are in contrast to the quarter of a wavelength displacement between streamlines and isotherms in the classical HRL solution.

It should be noted that *Figure* 7 illustrate cases that are comprised of two or three full flow cells. In fact, the cell width is not constant for the present set of boundary conditions, as earlier reported in the RT paper. Constant cell width is usually the case with known solutions for the onset of convection in 2D rectangular boxes, but the RT model is an exception. The rectangular box studied by Rees and Tyvand [8], shows a one-way wave with continuously varying wavelength being repeatedly generated at $x = 0$ to be advected out

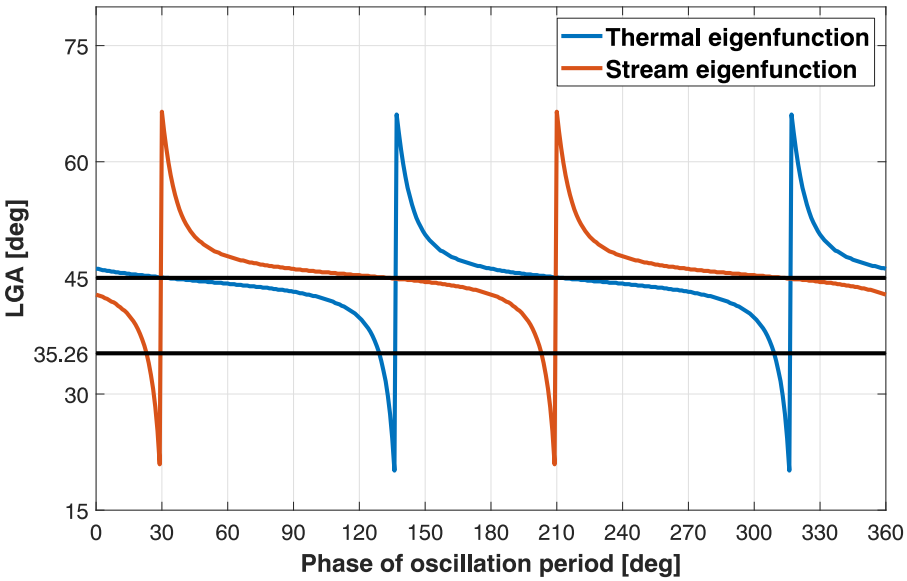


**Fig. 5** LGA as a function of oscillation phase at the origin, for the lowest eigenvalue of the thermal and stream eigenfunctions. Aspect ratio $L = 2$, Rayleigh number $R = 36.553$ and $\omega = 1.155$.

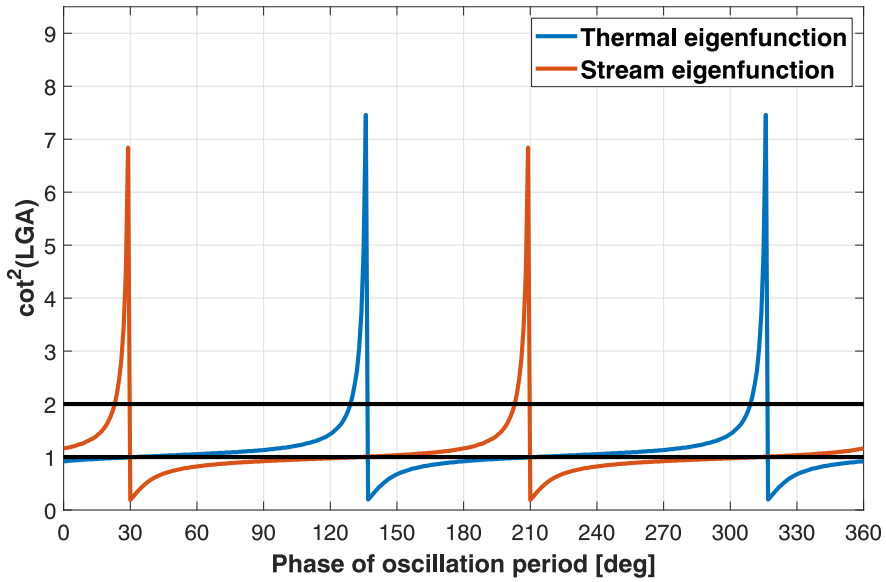


**Fig. 6** The LGA exponent $n = cot^2(\gamma)$ as a function of phase of oscillation at the origin, for lowest eigenvalue of the thermal and stream eigenfunctions. Aspect ratio $L = 2$, Rayleigh number $R = 36.553$ and $\omega = 1.155$.

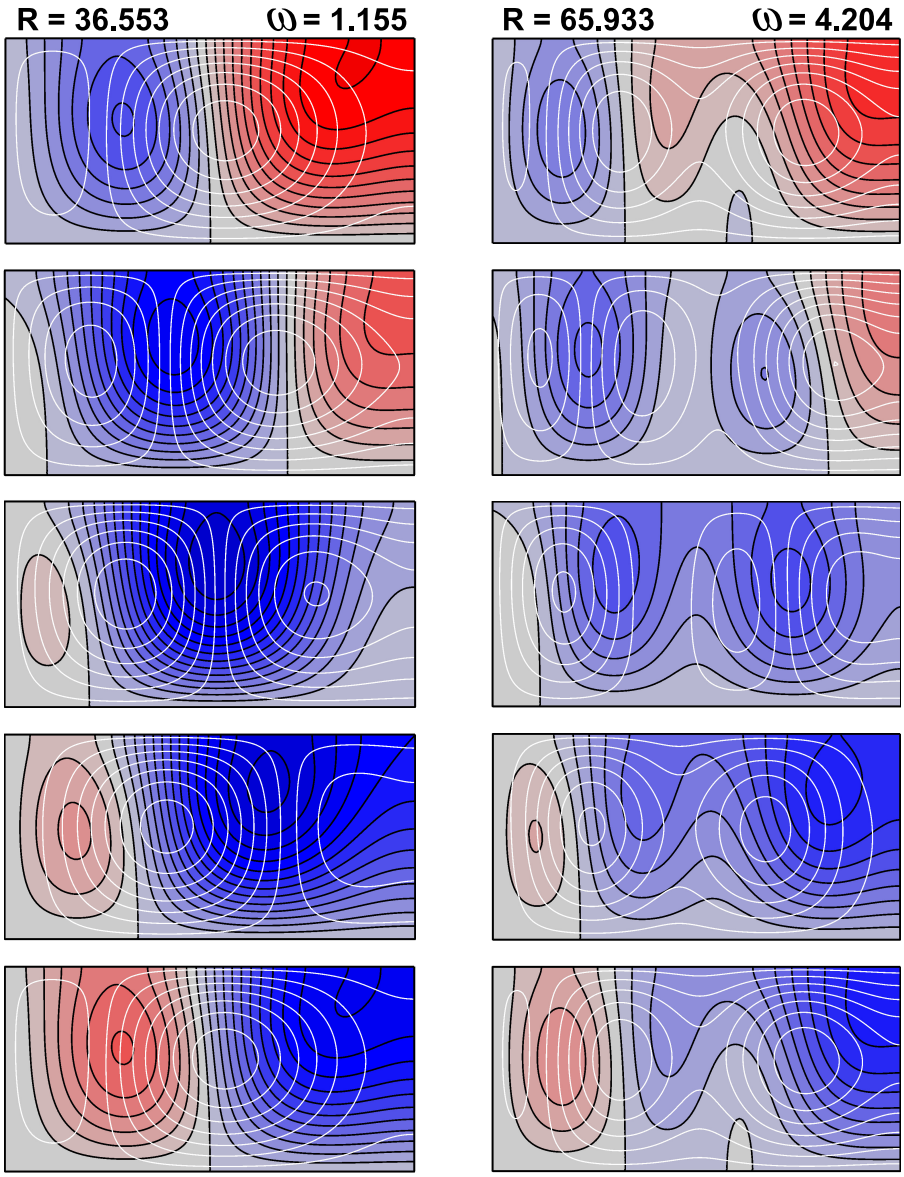


**Fig. 7** Streamlines (white) and isotherms (black) at equally spaced time intervals over one-half of a period for convection in a wide rectangle (aspect ratio $L = 2$) for the 2 first eigenfunctions. Time increases from the top to the bottom.

**Table 1** Comparison of Rayleigh numbers and oscillations frequencies in non-normal mode

| Eigenvalue | $L = 0.5$ | $L = 1.0$ | $L = 1.5$ | $L = 2.0$ |
|---|---|---|---|---|
| $R_1$ | 136.76 | 60.490 | 43.025 | 36.533 |
| $\omega_1$ | 41.681 | 7.3189 | 2.5046 | 1.1549 |
| $\log_{10}(\omega_1)$ | 1.6199 | 0.8644 | 0.3987 | 0.0625 |
| $R_2$ | 262.32 | 172.74 | 94.928 | 65.933 |
| $\omega_2$ | 31.858 | 28.513 | 9.3835 | 4.2043 |
| $\log_{10}(\omega_2)$ | 1.5032 | 1.4550 | 0.9724 | 0.62 |
| $R_3$ | 457.38 | 284.10 | 149.66 | 115.75 |
| $\omega_3$ | 26.046 | 18.267 | 1.6446 | 8.9572 |
| $\log_{10}(\omega_3)$ | 1.4157 | 1.2617 | 0.2161 | 0.95217 |
| $R_4$ | 547.20 | 360.78 | 182.16 | 142.23 |
| $\omega_4$ | 147.48 | 58.05 | 20.242 | 0.70917 |
| $\log_{10}(\omega_4)$ | 2.1687 | 1.7638 | 1.3063 | -0.1492 |
| $R_5$ | 726.95 | 355.33 | 201.48 | 171.89 |
| $\omega_5$ | 21.813 | 3.8473 | 6.1839 | 2.6892 |
| $\log_{10}(\omega_5)$ | 1.3387 | 0.5852 | 0.7913 | 0.4296 |

of the porous rectangle at $x = L$. This behavior occurs because of the mutual asymmetry between the thermomechanical conditions at $x = 0$ and those at $x = L$.

Table I summarizes the case studies with an overview of the Rayleigh number and the oscillation frequency for different aspect ratios and different eigenfunctions in non-normal mode.

### *3.2.4 Critical Rayleigh number as function of aspect ratio*

*Figure* 9 presents the Rayleigh number graphs of the two lowest onset modes, showing how they vary with aspect ratio $L$. They are compared with the benchmark case of normal-mode Rayleigh numbers. The critical Rayleigh number diverges in the limit $L \to 0$, as in the RT problem. In the opposite limit $L \to \infty$, our critical Rayleigh number for the preferred (lowest) onset mode tends toward the asymptotic limit $R = 27.10$, known from Nield [5], while the corresponding asymptotic limit for the RT problem is $R = 4\pi^2$ (Horton and Rogers [1]).

### *3.2.5 Critical oscillation frequency as function of aspect ratio*

*Figure* 10 presents the critical oscillation frequencies of the two lowest onset modes, showing how they vary with aspect ratio $L$. The benchmark normal-mode case is compared with the non-normal-mode frequencies. First we note that the oscillation frequencies tend to infinity as $L \to 0$, both in the present case and in the RT model. This infinite-frequency limit follows from a simple argument of dimensional analysis. The oscillations in a narrow rectangular box will then have $l^2/\kappa_m$ as their physical time scale, since the oscillations express a communication between the two vertical walls $CO$ and $AB$. Thus a different time scale replaces the assumed time scale $h^2/\kappa_m$ according to

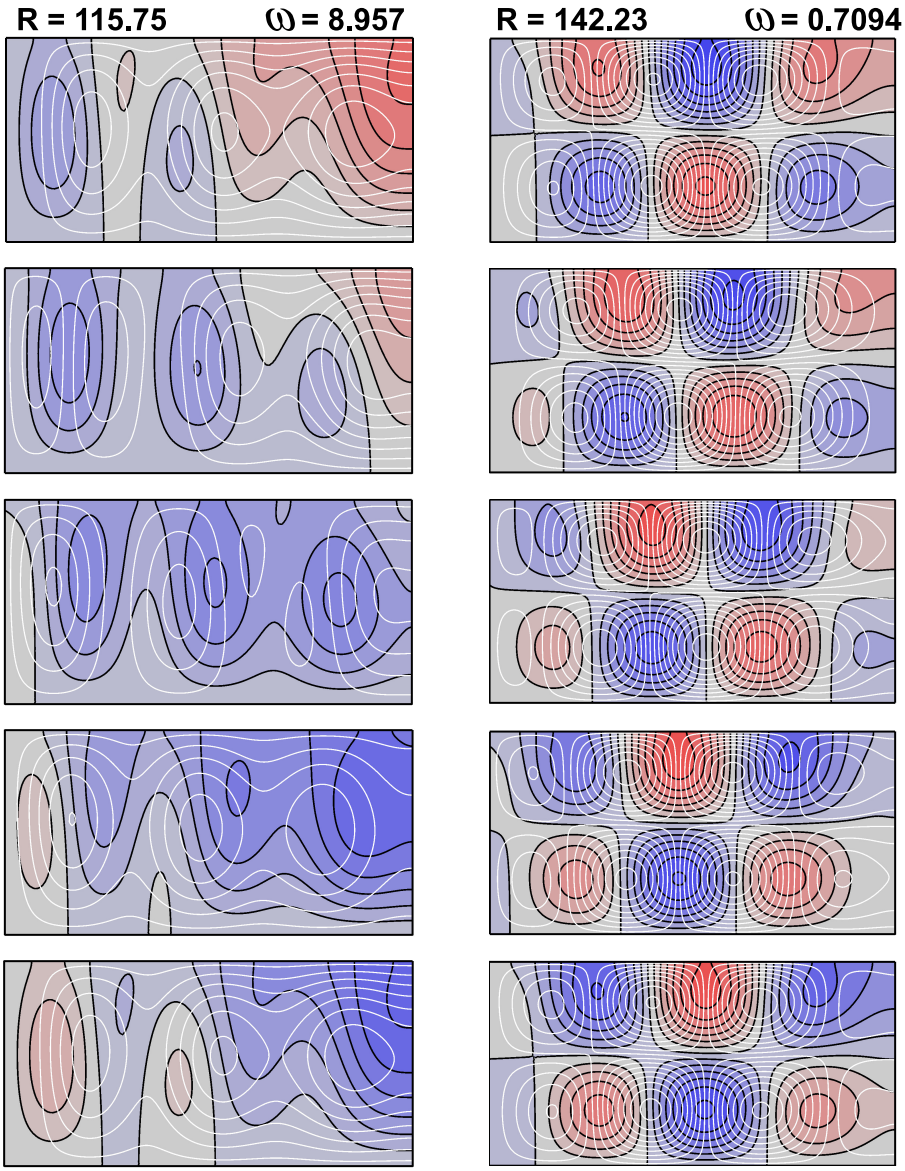


**Fig. 8** Streamlines (white) and isotherms (black) at equally spaced time intervals over one-half of a period for convection in a square (aspect ratio $L = 2$) for the third and the fourth eigenfunction. Time increases from the left to the right.

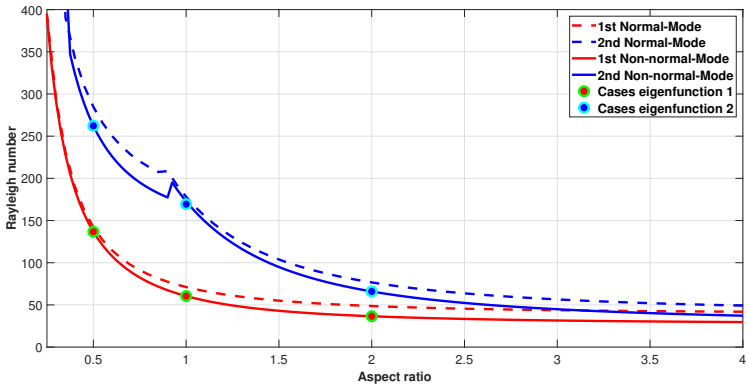


**Fig. 9** Two lowest Rayleigh numbers at marginal stability as a function of aspect ratio (L) in comparison with benchmark Normal-Mode. The filled circles refer to the cases displayed in *Figures* $3-6$. A numerical search generates continuous curves with a 0.025 resolution for the aspect ratio (L).

the dimensionless description. The time scale for $\omega$ that is assumed in the low aspect ratio limit of *Figure* 9 is therefore much smaller than the one implicitly assumed, being reduced by a factor $l^2/h^2 = L^2$ when $L \ll 1$. Smaller time scale of oscillations implies quicker oscillations, which explains why the dimensionless oscillations frequencies go to infinity as $L \to 0$ in *Figure* 10. Our only asymptotic estimate for the oscillations in the wide rectangle limit is the obvious leading-order limit, that the oscillations vanish in the limit $L \to \infty$, known from Nield [5].

### *3.2.6 Swapping between different modes*

*Figure* 11 shows that the modes experience slight jumps in the Rayleigh number as a function of the aspect ratio in the numerical search. The jumps happen at the intersection points where two different eigenfunctions meet, and where a new eigenfunction takes over as the $n^th$ lowest Rayleigh number.

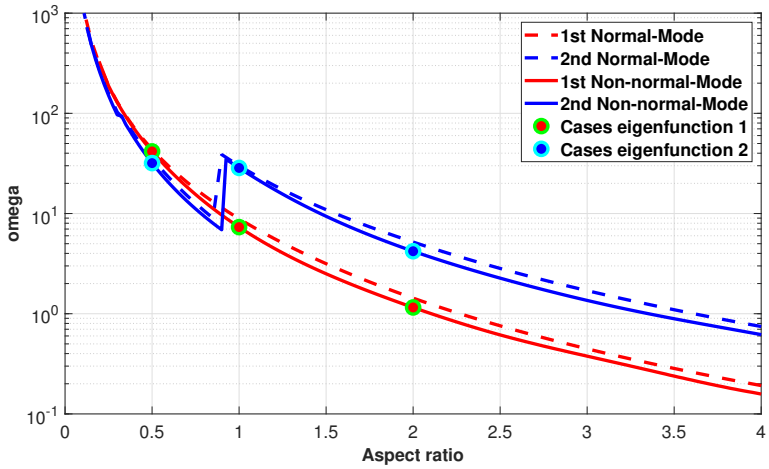


**Fig. 10** Oscillatory frequency at marginal stability as a function of aspect ratio (L) in comparison with benchmark Normal-Mode. The filled circles refer to the cases displayed in *Figures* 3 − 6. A numerical search for the two lowest Rayleigh numbers generates continuous curves with a 0.025 resolution for the aspect ratio (L).

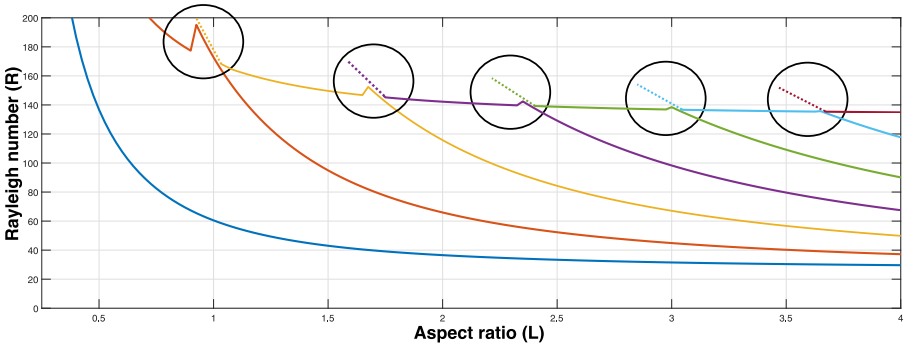


**Fig. 11** Illustration of slight jumps in the six lowest Rayleigh numbers with a 0.025 resolution for the aspect ratio (L).

## 4 Summary and conclusions

The mathematical theory of fourth-order eigenvalue problems is not very well developed in comparison with the harmonic analysis of second-order problems. The linearized Darcy-Bénard problem of convection onset (the HRL problem) in porous enclosures is one of the simplest fourth-order eigenvalue problems describing dissipative processes. The present work couples two causes for complexity that are not included in the classical HRL problem.

– An oscillatory onset mode of convection, due to an asymmetry between the left-hand and right-hand walls, none of which are compatible with normal modes.

– Boundary conditions incompatible with normal modes also at the upper boundary of the rectangular porous enclosure.

Thus we have designed an eigenvalue problem with boundary conditions incompatible with normal modes both horizontally and vertically, resulting in a complexity in eigenfunctions beyond the known HRL solutions from the literature. The critical Rayleigh number and the associated angular frequency of oscillation are not far away from the results for the benchmark RT problem (Rees and Tyvand [8]). At the large aspect ratio limit, vanishing oscillations reproduce two different but known onset problems solved by Nield [5].

Genuine differences between the present oscillatory problem and the RT problem appear in the local thermo-mechanical eigenfunctions. The RT problem does not possess a wave number parameter, but there is a spatially varying cell width. As a contrast, no wave number exists in the present problem. There is not even a clear notion of cell walls, and the cells change their shapes during their propagation through the porous cavity.

The present work reveals some of the little known inherent complexities of a genuinely fourth-order eigenvalue problem without degeneracies. Our choice of thermomechanical boundary conditions for the rectangular geometry give two corners that allow local expansions for the eigenfunctions. We have introduced the concept of LGA (Local Gradient Angle), for condensing information from the numerical solution. It is particularly useful near corners where both the eigenfunctions satisfy Dirichlet conditions. Two other corners of the rectangle have conflicting conditions for the walls that meet there. It is likely that the thermo-mechanical eigenfunctions have mild (integrable) singularities in these two corners, posing analytical challenges that are left for future work.

## References

1. Horton, C.W. and Rogers, F.T. (1945) Convection currents in a porous medium. J. Appl. Phys. **16**, 367-370.
2. Lapwood, E.R. (1948) Convection of a fluid in a porous medium. Proc. Camb. Phil. Soc. **44**, 508-521.
3. Tyvand, P.A. and Storesletten, L. (2018) Degenerate onset of convection in vertical porous cylinders. J. Eng. Math. 113, 165-181.
4. Tyvand, P.A., Nøland, J.K. and Storesletten, L. (2019) A non-normal-mode marginal state of convection in a porous rectangle. Transp. Porous Med. **128**, 633-651.
5. Nield, D.A. (1968) Onset of thermohaline convection in a porous medium. Water Resources Res. **11**, 553-560.
6. Beck, J.L. (1972) Convection in a box of porous material saturated with fluid. Phys. Fluids **15**, 1377-1383.
7. Nilsen, T. and Storesletten, L. (1990) An analytical study on natural convection in isotropic and anisotropic porous channels. ASME J. Heat Transf. **112**, 396-401.
8. Rees, D.A.S. and Tyvand, P.A. (2004a) Oscillatory convection in a two-dimensional porous box with asymmetric lateral boundary conditions. Phys. Fluids 16, 3706-3714. Referred to in the text as the RT paper.
9. Nygård, H.S. and Tyvand, P.A. (2010) Onset of convection in a porous box with partly conducting and partly penetrative sidewalls. Transp. Porous Med. **84**, 55-73.
10. Barletta, A. and Storesletten, L. (2015) Onset of convection in a vertical porous cylinder with a permeable and conducting side boundary. Int. J. Therm. Sci. **97**, 9-16.

11. Rees, D.A.S. and Tyvand, P.A. (2004b) The Helmholtz equation for convection in two-dimensional porous cavities with conducting boundaries. J. Eng. Math. 490, 181-193.
12. Storesletten, L. and Tveitereid (1991) Natural convection in a horizontal porous cylinder. Int. J. Heat Mass Transf. 34, 1959-1968.
13. Rees, D.A.S. and Lage, J.L. (1996) The effect of thermal stratification on natural convection in a vertical porous insulation layer. Int. J. Heat Mass Transf. 40:111-121.